



Isotope shifts for $^1S_0 - ^3P_{0,1}^o$ Yb lines from multiconfiguration Dirac-Hartree-Fock calculations

Jesse S. Schelfhout * and John J. McFerran †

Department of Physics, University of Western Australia, 35 Stirling Highway, Crawley, Western Australia 6009, Australia



(Received 12 March 2021; accepted 20 July 2021; published 10 August 2021)

Relativistic multiconfiguration Dirac-Hartree-Fock calculations with configuration interaction are carried out for the 1S_0 and $^3P_{0,1}^o$ states in neutral ytterbium by use of the available GRASP2018 package. From the resultant atomic state functions and the RIS4 program, we evaluate the mass- and field-shift parameters for the $^1S_0 - ^3P_0^o$ (clock) and $^1S_0 - ^3P_1^o$ (intercombination) lines. We present improved estimates of the nuclear charge parameters $\lambda^{A,A'}$ and differences in mean-square charge radii $\delta\langle r^2 \rangle^{A,A'}$ and examine the second-order hyperfine interaction for the $^3P_{0,1}^o$ states. Isotope shifts for the clock transition have been estimated by three largely independent means from which we predict the unknown clock-line frequencies in bosonic Yb isotopes. Knowledge of these line frequencies has implications for King-plot nonlinearity tests and the search for beyond-standard-model signatures.

DOI: [10.1103/PhysRevA.104.022806](https://doi.org/10.1103/PhysRevA.104.022806)

I. INTRODUCTION

Atomic systems offer a means to test fundamental physics at a high level of precision in the search for phenomena beyond the standard model (SM) of elementary particles [1–3]. This may be undertaken by examining King plots that are generated through isotope-shift spectroscopy of at least two transitions in an atomic species [4–7]. Nonlinearities in such plots may arise due to higher-order effects within the SM, such as higher-order mass shifts [8,9], nuclear deformation [10,11], and nuclear polarizability [12], or due to phenomena beyond the SM [5–7,12–16]. Accurate atomic structure calculations are needed to explore possible causes for such nonlinearities, as is done by investigating additional contributions to isotope shifts beyond the simple mass shift and field shift [4,5,11,12,17]; this can be done by analyzing the residuals of a linear fit to a King plot, whereby different nonlinearities are expected to have different signatures in the residuals [4]. Such calculations can also be used in the extraction of information about the nuclear structure [18,19].

The recent work of Counts *et al.* [4], using narrow optical quadrupole transitions in Yb^+ , is one of the only King plots to date which demonstrates nonlinearity beyond the level of experimental uncertainty. This 3σ nonlinearity is consistent with interpretations as either higher-order SM effects or physics beyond the SM. Linearity of the Ca^+ King plot in Ref. [20] suggests that its interpretation as higher-order SM effects should be favored [17]. Recent work by Allehabi *et al.* [11] suggests that nuclear deformation in Yb nuclei can produce a King-plot nonlinearity at a level consistent with that found in Ref. [4]. A means of exploring the dominant cause of King-plot nonlinearity is by combining prior Yb^+ data with isotope-shift measurements of the $^1S_0 - ^3P_0^o$ transition

in neutral Yb. In this work we provide estimates of these clock-transition frequencies for all the stable bosonic isotopes of Yb I, aiding the experimental search for these lines.

Advances in modern computing allow for relativistic atomic structure calculations to be performed with results consistent with experimentally determined values to a few parts in 10^5 [21–24]. Such computations are also used to determine mass- and field-shift parameters of isotope shifts for King-plot analyses [4,10,20,25–28]. Low-lying energy levels in ytterbium have been explored through computational means [29–43]; however, they usually do not compute isotopes separately and often omit the $^3P_0^o$ state. In this paper, the isotope shifts of the clock and intercombination-line (ICL) transitions are computed *ab initio*, and the mass- and field-shift parameters that aid King-plot analysis are calculated.

We describe our computational procedure in Sec. II, where the atomic state function is refined through a restricted active set approach using multiconfiguration Dirac-Hartree-Fock (MCDHF) and configuration interaction (CI) computations from a multireference set of configuration state functions. Section III summarizes the energy-level differences and isotope shifts resulting from the MCDHF-CI computations. Section IV gives a detailed account of the mass- and field-shift parameters that are evaluated with RIS4 using the calculated atomic state functions. The second-order hyperfine interaction is discussed in Sec. V, which is necessary to account for the shift in centroid frequencies for the fermionic isotopes. The nuclear charge parameters are evaluated in Sec. VI, followed by a King-plot analysis and estimates of the clock-line isotope shifts in Sec. VII. Additional information, including the predictions of the absolute clock-line frequencies, is given in the Appendixes.

II. COMPUTATIONAL METHOD

Most *ab initio* isotope-shift computations perform computations for a single isotope and then calculate the mass- and

*jesse.schelfhout@uwa.edu.au

†john.mcferran@uwa.edu.au

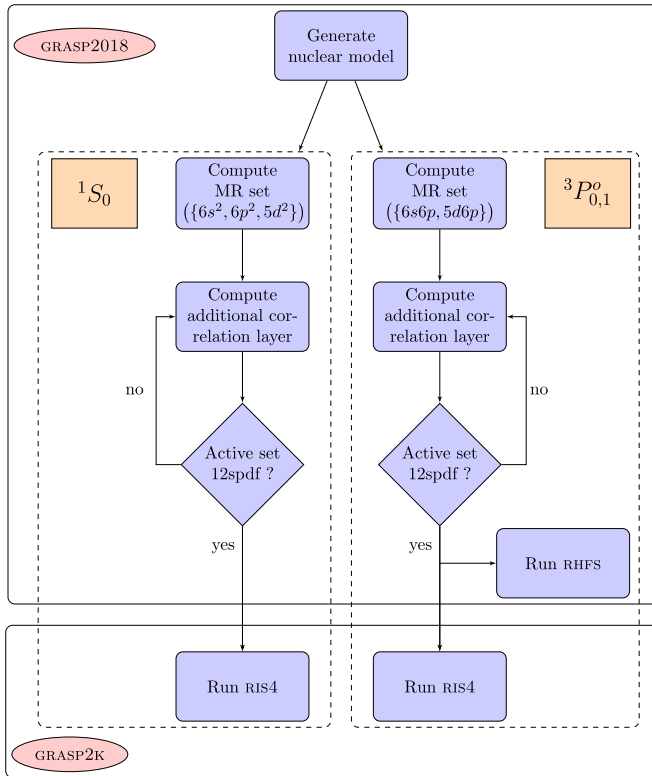


FIG. 1. Procedure for performing MCDHF-CI computations (GRASP2018) and extracting isotope-shift information (GRASP2K). Correlation layers are added until $n = 12$ for ground and excited states. Mass- and field-shift parameters are evaluated with the RIS4 package. MR, multireference; RHFS, relativistic hyperfine-structure program [47].

field-shift parameters, using nuclear charge parameters $\lambda^{A,A'}$ derived from experiment to arrive at isotope shifts. In contrast, the computations presented here are similar to the “exact” method of [19] and to those of [44,45], in that energies and wave functions are computed for each isotope of interest, and the isotope shifts are taken as the differences between these energies. It is suggested that this approach can be strongly model dependent [46], so the more common method of calculating isotope shifts via computed mass- and field-shift parameters is also pursued in Secs. IV and VII.

A two-step approach is used to estimate the isotope shifts and mass-shift and field-shift parameters for the clock and intercombination transitions using computational methods. First, a MCDHF-CI approach is used to compute the atomic state functions (ASFs) for the 1S_0 ground state and $^3P_{0,1}$ excited states using the FORTRAN 95 package GRASP2018 (General Relativistic Atomic Structure Package) [47]. Isotope shifts are calculated as the differences in energy between the ground and excited states for different isotopes. Mass- and field-shift parameters are then extracted using the FORTRAN 90 program RIS4 (Relativistic Isotope Shift) [46]. RIS4 was written as an addition to the GRASP2K package [48]; however, we have been able to use it in conjunction with GRASP2018 [49]. The computational process is outlined in Fig. 1 with further explanation below. A MCDHF-CI approach is used in favor of other approaches, e.g., configuration interaction

TABLE I. Multireference configurations for the clock- and intercombination-transition levels in Yb I.

Level	J^Π	MR configurations	N_{CSFs}
$6s^2 \ ^1S_0$	0^+	$[\text{Kr}]4d^{10}4f^{14}5s^25p^6 + \{6s^2, 6p^2, 5d^2\}$	5
$6s6p \ ^3P_0^o$	0^-	$[\text{Kr}]4d^{10}4f^{14}5s^25p^6 + \{6s6p, 5d6p\}$	2
$6s6p \ ^3P_1^o$	1^-	$[\text{Kr}]4d^{10}4f^{14}5s^25p^6 + \{6s6p, 5d6p\}$	5

with many-body perturbation theory (CI+MBPT) [10,50], all-order methods [51], and relativistic coupled-cluster calculations [52], due to the recent updates of the GRASP and RIS packages and their cross compatibility allowing for ease of extraction of isotope-shift parameters.

A restricted-active-space approach is used to construct the atomic state functions, whereby a multireference (MR) set is chosen, and additional configuration state functions (CSFs) are systematically included according to rules for allowed substitutions. The ground-state electron configuration for ytterbium is $[\text{Xe}]4f^{14}6s^2$. The MR set for the 1S_0 ground state is thus taken to be $[\text{Xe}]4f^{14}\{6s^2, 5d^2, 6p^2\}$ as these are the configurations with two valence electrons which can form 1S_0 terms and are near in energy to the $6s^2$ ground state. This is the same MR set as that of the “MCDF IV” approach used in Ref. [53]. The excited states $^3P_{0,1}^o$ have electron configuration $[\text{Xe}]4f^{14}6s6p$. Conveniently, they can be computed simultaneously using the extended optimal level (EOL) mode of the RMCDHF(_MPI) program [47]. Computing the $^3P_0^o$ and $^3P_1^o$ excited states together using the EOL mode is found to have a negligible effect on the clock-transition frequency compared with computation of the $^3P_0^o$ state on its own ($\sim 0.3\%$ difference). The MR set for $^3P_{0,1}^o$ is taken to be $[\text{Xe}]4f^{14}\{6s6p, 5d6p\}$. The MR sets are summarized in Table I, where N_{CSFs} is the number of configuration state functions for the MR set when using relativistic orbital labeling.

Correlation orbitals are added layer by layer, where a layer includes orbitals for each angular momentum value allowed for the substitutions (e.g., $7s, 7p_-, 7p_+, 6d_-, 6d_+, 5f_-, 5f_+$, with the subscripts $+$ and $-$ indicating $j = l \pm 1/2$). Correlation layers are truncated at a principal quantum number of 12 [54], leaving the active space at $12sp11d10f$, and partial layers are added to bring the final active space to $12spdf$. The new correlation orbitals are optimized using the self-consistent field procedure [55] while leaving the previously computed orbitals invariant. The correlation layers are built using single and restricted double (SrD) substitutions from configurations in the MR set. The closed core is taken to be $[\text{Kr}]4d^{10}$. The restriction for the SrD substitutions is substitution of at most one electron from the set of available core orbitals ($4f_{\pm}, 5s, 5p_{\pm}$). This keeps the computations tractable while allowing a considerable degree of valence-valence and core-valence correlation. The number of CSFs grows to 30 256, 30 668, and 84 519 for 1S_0 , $^3P_0^o$, and $^3P_1^o$, respectively [56]. The dominant CSFs by percentage contribution to the total ASF for each state are tabulated in Appendix B.

For each energy level, the atomic state function computed with all the desired correlation layers is corrected for higher-order QED effects through the RCI_MPI program before

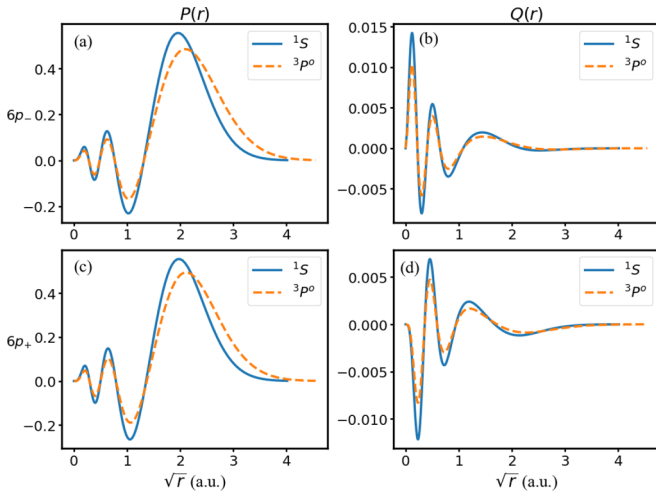


FIG. 2. Large, $P(r)$, and small, $Q(r)$, component radial wave functions for the 1S_0 (solid blue lines) and $^3P_{0,1}^o$ (dashed orange lines) states computed using GRASP2018. The abscissa is \sqrt{r} , where r is the distance from the center of the nucleus in atomic units. (a) $P(r)$ for the $6p_-$ orbital. (b) $Q(r)$ for the $6p_-$ orbital. (c) $P(r)$ for the $6p_+$ orbital. (d) $Q(r)$ for the $6p_+$ orbital.

computing any observables. The transverse photon interaction is reduced to the Breit interaction by scaling all transverse photon frequencies by a factor of 10^{-6} [47]. Vacuum polarization effects are accounted for, and self-energy is estimated for orbitals up to $n = 6$. The normal and specific mass shifts due to the nuclear recoil are also included in the CI computations. Ytterbium nuclei are known to be deformed [11,57,58]; however, the nuclear model used for these computations (see Appendix A) does not account for nuclear deformation.

The wave function arising from a single CSF is an antisymmetric product of one-electron wave functions [59] in the form of a Slater determinant [60]. The radial functions for the $6p_-$ and $6p_+$ orbitals resulting from our MCDHF-CI computations for the 1S_0 and $^3P_{0,1}^o$ states are represented in Fig. 2, where the large-component, $P(r)$, and small-component, $Q(r)$, radial functions are presented separately. Less significant deviations between the ground-state and excited-state radial functions were found for the $6s$ orbital.

Where possible, uncertainties in the presented computational results are estimated by direct comparison with experiment [61]. In other cases, uncertainties are estimated by systematically adding correlation layers or increasing the size of the core available for correlation and analyzing the convergence of the desired properties [55]. We use a combination of these methods, with quoted uncertainties corresponding to 1σ unless otherwise stated. The latter approach may not include systematic uncertainties arising from the MCDHF-CI method, and so it is desirable to compare it against other computational approaches [62,63].

The efficacy of MCDHF-CI computations was demonstrated recently; for example, Zhang *et al.* [64] calculated energies for sulfurlike tungsten with near-spectroscopic accuracy; Silwal *et al.* [44] computed isotope shifts within the uncertainty bounds of experimental results in Mg-like and Al-like systems, and Palmeri *et al.* [65] produced isotope shifts in reasonable agreement with experimental results for osmium.

Froese Fischer and Senchuk [66] noted that good accuracy is generally achieved for light elements or highly ionized heavy elements but suggested neutral heavy elements with open core subshells can be subject to problems with the accuracy of the calculations or with the energies of states not being resolved. These problems are not expected to strongly influence the results of this paper due to the simple closed-shell electron configuration of neutral ytterbium, in particular the closed $4f^{14}$ subshell.

Further, neglecting core-core correlations here is justified: The agreement between computational and experimental values for oscillator strength in singly ionized thallium, a heavier system than ytterbium with an additional closed $5d$ subshell, was found to be better in the absence of core-core correlation [67]. MCDHF computations for magnesium were found to result in more accurate isotope shifts in the absence of core-core correlation [68]; the “errors” in the normal and specific mass shifts “accidentally” canceling is not concerning since only the total mass shift can be comparable to observation [69]. Core-core correlation was not included in MCDHF computations of neutral zinc, a smaller system than ytterbium with closed core subshells and two valence electrons, due to the magnitude of the calculations [69].

Various extensions to the correlation model used in this paper were investigated, including core-core correlation, deeper core-valence correlation, single and restricted double and triple substitutions, and the inclusion of g orbitals. Any of these models that improved upon the accuracy of either the calculated absolute transition frequencies, the isotope shifts, the nuclear charge parameters, or the hyperfine-structure constants reduced the agreement between computational and experimental values for the other quantities. It is possible that an active space accounting for deeper core-core correlation than investigated, which would lead to more CSFs than feasible with available computational resources, would produce more accurate results.

The majority of the computations were performed at the University of Western Australia High Performance Computing Centre on Kaya [70], one of their high-performance computing machines [71]. Kaya comprises Dell PowerEdge R740 nodes, each with two Intel Xeon Gold 6254 processors with 18 cores, 768 GB of RAM, and 3.2 TB of nonvolatile memory. Thirty-four cores on one node were utilized for the computations.

III. RESULTS: TRANSITION FREQUENCIES AND ISOTOPE SHIFTS

The computed energy-level differences are presented in Table II for the clock transition and in Table III for the ICL transition. Energies computed in atomic units (E_h) are converted into frequencies in hertz via multiplication by $2cR_\infty = 6.579683920502(13) \times 10^{15} \text{ Hz } E_h^{-1}$ [72]. The computed energy-level differences are 0.8% larger than the experimental values for the clock transition and 0.7% larger for the ICL transition.

For the clock transition, the isotope shift between ^{173}Yb and ^{174}Yb is calculated as -615 MHz , and that between ^{171}Yb and ^{173}Yb is calculated as -1389 MHz . Experimentally, these values are found using data from Refs. [73–76]

TABLE II. Computed energy-level separations and isotope shifts for the 1S_0 ground state and $^3P_0^o$ excited state for stable isotopes of Yb. Isotope shifts are relative to ^{176}Yb .

Isotope	Energy separation (MHz)	Isotope shift (MHz)
168	522 679 368	-5073
170	522 677 872	-3577
171	522 677 352	-3057
172	522 676 461	-2166
173	522 675 963	-1668
174	522 675 348	-1053
176	522 674 295	0

to be $-551.536050(11)$ and $-1259.745595(11)$ MHz, corresponding to percentage differences of 11.5% and 10.3%, respectively. Both computed isotope shifts are larger in magnitude than the experimental values. We expect that the isotope shifts presented in Table II all have an error of approximately 11%. The computed isotope shifts for the intercombination line are presented in Table III. These values differ, on average, by 11.5% when compared with measured values from Ref. [77]. These differences may reduce with the inclusion of deeper core-valence correlations [27,47,67]. Investigation of deeper core-valence correlation effects led to isotope-shift values with $\sim 6\%$ difference from experimental values for an active core down to $4s$, but the values for the absolute transition frequencies, hyperfine-structure constants, and nuclear charge parameters had larger discrepancies with experimental results than the model adopted for the results in this paper. Extending the active core even deeper did not improve this situation. Variation in nuclear deformation between the isotopes, not accounted for in these computations, may also contribute to the differences between the experimental and computational isotope shifts. While these differences are a concern, they do not prevent us from making viable predictions for clock-transition frequencies in the bosonic isotopes: The mass- and field-shift factors determined from these calculations (see Sec. IV) lead to nuclear charge parameters consistent with previous results (see Sec. VI) and reliable isotope-shift estimates can be made with the aid of some experimental data (see Sec. VII).

IV. MASS- AND FIELD-SHIFT PARAMETERS

The differences in nuclear mass and charge distributions between isotopes of the same element give rise to small vari-

TABLE III. Computed energy-level separations and isotope shifts for the 1S_0 ground state and $^3P_0^o$ excited state for stable isotopes of Yb. Isotope shifts are relative to ^{176}Yb .

Isotope	Energy separation (MHz)	Isotope shift (MHz)
168	543 180 934	-5127
170	543 179 422	-3615
171	543 178 897	-3090
172	543 177 997	-2190
173	543 177 493	-1686
174	543 176 872	-1065
176	543 175 807	0

ations in the energy eigenvalues for the atomic system, i.e., isotope shifts. By convention, the isotope shift for a pair of isotopes is calculated by subtracting the energy of the lighter isotope from that of the heavier isotope [78], so for isotopes A and A' with $m_A > m_{A'}$, the isotope shift is given by

$$\delta v^{A,A'} = v^A - v^{A'}. \quad (1)$$

To a very good approximation, an isotope shift may be split into a mass shift and a field shift, arising from differences in the nuclear recoil and nuclear charge distribution, respectively, between the isotopes [78]. Under the approximation that the electronic wave function for a particular state is invariant between isotopes, the mass and field shifts for an atomic state, denoted by i , factor into electronic and nuclear components

$$\delta v_i^{A,A'} = K_i \mu^{A,A'} + F_i \lambda^{A,A'}, \quad (2)$$

where K_i (F_i) is the electronic mass- (field-) shift factor,

$$\mu^{A,A'} = \frac{1}{m_A} - \frac{1}{m_{A'}} \quad (3)$$

is the nuclear mass parameter, and

$$\lambda^{A,A'} = \sum_{n \geq 1} C_n \delta \langle r^{2n} \rangle^{A,A'} \quad (4)$$

is the nuclear charge parameter, where C_n are Seltzer's coefficients [42,79,80]. For a transition α between an upper state j and a lower state i , the isotope shift is given by

$$\delta v_\alpha^{A,A'} = \delta v_j^{A,A'} - \delta v_i^{A,A'} = K_\alpha \mu^{A,A'} + F_\alpha \lambda^{A,A'}, \quad (5)$$

where $K_\alpha = K_j - K_i$ and $F_\alpha = F_j - F_i$.

To first order, the electronic mass- and field-shift parameters are isotope independent; however, higher-order effects lead to isotope dependence through the subtle differences in the electronic wave functions between isotopes [17]. Accordingly, the mass- and field-shift factors have been evaluated for each isotope for both the clock and ICL transitions using the RIS4 program following computation of the wave functions using GRASP2018. We present the values for the field-shift factors in Table IV, where we see slight isotope dependence. The mean values across all seven stable isotopes are $F_{\text{clock}} = -10.848(21)$ GHz fm $^{-2}$ and $F_{\text{ICL}} = -10.951(21)$ GHz fm $^{-2}$; we comment on the uncertainties below. For the clock transition, a previously reported value of F_{clock} was calculated via AMBIT [50], using only configuration interaction (without MBPT) and a correlation model very similar to this work [17]. For the intercombination line, the mean value is compared with previous evaluations of F_{ICL} at the bottom of Table IV. Our value lies approximately central to the range of previous estimations, but with higher precision.

The mass-shift factors K experience little change with isotope; the mean values are $K_{\text{clock}} = -288(75)$ GHz u and $K_{\text{ICL}} = -280(72)$ GHz u. Note the values are negative. A negative specific mass shift for 3P states for two-electron spectra is suggested to arise from angular correlation (according to a private communication in Ref. [39]). While these negative mass shifts appear to be at odds with the positive value of $K_{\text{ICL}} = 1.5(5)$ THz u found in Ref. [82], a review of their formulas reveals a difference in sign for the nuclear mass

TABLE IV. Electronic field-shift factor F for the $^1S_0 - ^3P_0^o$ clock transition and the $^1S_0 - ^3P_1^o$ intercombination line (ICL).

Isotope	F_{clock} (GHz fm $^{-2}$)	F_{ICL} (GHz fm $^{-2}$)
168	-10.865(18)	-10.969(18)
170	-10.855(18)	-10.959(18)
171	-10.852(18)	-10.955(18)
172	-10.846(18)	-10.950(18)
173	-10.843(18)	-10.947(18)
174	-10.839(18)	-10.943(18)
176	-10.833(18)	-10.936(18)
Mean	-10.848(21)	-10.951(21)
Ref. [17]	-9.7192	
Ref. [81]		-9.3(2.1)
Ref. [58]		-10.9 ^a
Ref. [82]		-12.3(0.2)
Ref. [83]		-12.2(0.7) ^a

^aValue is positive in reference (assumed to be absolute value)

parameter. The same convention ($\mu^{A,A'} > 0$ for $m_A > m_{A'}$) is used in [58,84]. The convention used in this work [Eq. (3)] is consistent with that of Refs. [46,81]. Berengut *et al.* determined $K_{\text{clock}} = -655$ GHz u using a CI+MBPT method [17], implemented via AMBIT [50], demonstrating the dependence of the calculation on the method and supporting its approximate magnitude and sign. The calculated mass-shift factor for the intercombination line is consistent with that of Ref. [81], and the field-shift factor is consistent with Refs. [58,81].

$$\begin{aligned} \langle (J-1)IFm_F | \mathcal{H}_{\text{hfs}} | JIFm_F \rangle &= \frac{1}{2}A(J, J-1)\sqrt{(K+1)(K-2F)(K-2I)(K-2J+1)} \\ &+ B(J, J-1)\frac{[(F+I+1)(F-I)-J^2+1]\sqrt{3(K+1)(K-2F)(K-2I)(K-2J+1)}}{2I(2I-1)J(J-1)} \end{aligned} \quad (7)$$

and

$$\langle (J-2)IFm_F | \mathcal{H}_{\text{hfs}} | JIFm_F \rangle = B(J, J-2), \quad (8)$$

where $K = I + J + F$.

Only isotopes ^{171}Yb and ^{173}Yb have nonzero nuclear spin and thus experience the hyperfine interaction. For $J = 1$, the off-diagonal electric quadrupole hyperfine-structure constant $B(^3P_1, ^3P_0)$ is vanishing. The diagonal and off-diagonal hyperfine-structure constants calculated using the RHFS program in the GRASP2018 package [47,86] are presented in Table V. Uncertainties are taken to be 4% by comparison of the diagonal hyperfine-structure constants with the experimental values from Atkinson *et al.* [77].

Calculation of the centroid shift using Eq. (6) makes use of the energy difference between the fine-structure levels, $^3P_0^o$ and $^3P_1^o$, i.e., the value of 21 092 574.882(93) MHz for ^{174}Yb based on measurements presented in Refs. [76,77]. The centroid shifts for the clock transition, to second order in perturbation theory, for the mixing of the $^3P_0^o$ and $^3P_1^o$ states we

Uncertainties in K and F for each isotope are estimated by systematically increasing the size of the computations. The convergence of the parameters as correlation layers are added for isotope ^{174}Yb and as the set of core orbitals available for core-valence correlation is extended for isotope ^{176}Yb is presented in Appendix C. The uncertainties for the mean values (over isotopes) are taken to be the sum by quadrature of (i) the standard deviation of the isotopic data and (ii) the estimated uncertainty for each isotope. We note that these uncertainty estimates do not account for possible systematic errors associated with the computational method, but we see below that they yield consistency with the ratio $F_{\text{ICL}}/F_{\text{clock}}$ from experimental data.

V. SECOND-ORDER HYPERFINE STRUCTURE

The off-diagonal second-order hyperfine interaction for isotopes with nuclear spin results in a shift of the centroid (center of gravity) of the hyperfine manifold relative to that of an isotope with no nuclear spin [41,85]. Correcting the experimentally determined centers of gravity for these shifts provides a means of comparison between the bosonic and fermionic isotopes (e.g., for King-plot analysis). The shift for a state denoted $|JIFm_F\rangle$ is given by

$$\Delta E_F^{(2)} = \sum_{J' \neq J} \frac{|\langle JIFm_F | \mathcal{H}_{\text{hfs}} | J'IFm_F \rangle|^2}{E_J - E_{J'}}. \quad (6)$$

The matrix element in Eq. (6) can be written in terms of the off-diagonal hyperfine-structure constants, $A(J, J')$ and $B(J, J')$, as

calculate to be $-0.537(44)$ and $-0.476(39)$ MHz for ^{171}Yb and ^{173}Yb , respectively. For the ICL, the $F = I$ hyperfine level is the only one influenced by mixing with the $^3P_0^o$ state, so the shift to its centroid is smaller. The new centroids for the ICL isotope shifts relative to ^{176}Yb are $-1510.948(42)$ MHz for ^{173}Yb and $-2781.182(54)$ MHz for ^{171}Yb (cf. Ref. [77]).

The centers of gravity for the intercombination-line isotope shifts presented in Ref. [77] are correct to first order in pertur-

TABLE V. Hyperfine-structure constants calculated using RHFS. $A(^3P_1)$ and $B(^3P_1)$ are the diagonal magnetic dipole and electric quadrupole hyperfine-structure constants, respectively, and $A(^3P_1, ^3P_0)$ is the off-diagonal magnetic dipole hyperfine-structure constant.

Isotope	$A(^3P_1)$ (GHz)	$A(^3P_1, ^3P_0)$ (GHz)	$B(^3P_1)$ (MHz)
171	4.07(17)	3.89(16)	0
173	-1.12(5)	-1.07(5)	-794(32)

TABLE VI. Isotope shifts $\delta\nu^{A,A'} = \nu^A - \nu^{A'}$ for the $^1S_0 - ^3P_0^o$ ICL and $^1S_0 - ^3P_0^o$ clock transitions in Yb I. For the fermionic isotopes, corrections to second order in the hyperfine interaction are taken into account, and the centroid for the hyperfine manifold is used for the ICL transition. These results are determined mostly from the experimental measurements found in Refs. [73–77].

A	A'	$\delta\nu_{\text{ICL}}^{A,A'}$ (MHz)	$\delta\nu_{\text{clock}}^{A,A'}$ (MHz)
176	174	−954.734(31)	
174	172	−1000.792(48)	
172	170	−1285.816(81)	
170	168	−1369.602(93)	
173	172	−444.578(56)	
172	171	−825.656(65)	
171	170	−460.160(91)	
174	173	−556.214(53)	−552.012(39)
173	171	−1270.234(69)	−1259.807(58)

bation theory; however, the second-order corrections due to mixing with the $^3P_0^o$ state are greater than the experimental uncertainty and so are accounted for here. The effects of mixing with other nearby states ($^1P_1^o$, $^3P_2^o$) are estimated to be below the level of experimental uncertainty. The centers of gravity determined from the measured clock-transition frequencies for ^{171}Yb [73,74] and ^{173}Yb [75] must also take into account the higher-order perturbations in order to make a comparison with that of ^{174}Yb [76] in a King-plot analysis. The resultant isotope shifts (between centers of gravity for the fermions) are presented in Table VI.

VI. NUCLEAR CHARGE PARAMETER

The nuclear charge parameter can be calculated by rearranging Eq. (5) to find

$$\lambda^{A,A'} = \frac{1}{F_\alpha} (\delta\nu_\alpha^{A,A'} - K_\alpha \mu^{A,A'}). \quad (9)$$

By use of the isotope shifts presented in Table VI, the mass-shift and field-shift parameters calculated in Table IV, and the isotope masses presented in Appendix A, the nuclear charge parameter $\lambda^{A,A'}$ can be determined from Eq. (9), as presented in Table VII. The uncertainties are dominated by the uncertainty in K , but they are lower than those of previous estimates by at least a factor of 4. King [78] notes that the values from Clark *et al.* [58] give excessive weight to the muonic and x-ray data in their combined analysis, which leads to larger values than our own. The fifth column in Table VII shows $\lambda^{A,A'}$ values from Clark *et al.* based on optical data alone, showing better agreement with our values. Jin *et al.* [83] assumed a specific mass shift of zero and used a field-shift parameter of larger magnitude (12.2 GHz fm^{−2}), leading to their lower values for $\lambda^{A,A'}$.

The nuclear charge parameter $\lambda^{A,A'}$ can be converted into the difference in mean-square nuclear charge radii $\delta\langle r^2 \rangle^{A,A'}$, through rescaling [81,82] or using an iterative procedure [84,87]. Fricke and Heilig [81] determined the higher-order moments contribute −5.9% to $\lambda^{A,A'}$ based on experimental data from muonic atoms, so the differences in mean-square charge radii are recovered in this work by rescaling via

TABLE VII. Nuclear charge parameters $\lambda^{A,A'}$ determined from the Yb I intercombination-line measurements and calculated F and K parameters (in units of 10^{−3} fm², third column). Data from prior works are presented for comparison.

A	A'	This work	Ref. [58] ^a	Ref. [58] ^b	Ref. [83]	Ref. [82]
176	174	88.86(47)	109(8)	87(13)	79.4(4.0)	86(2)
174	172	93.10(48)	114(8)	92(15)	83.3(4.2)	90(2)
172	170	119.17(51)	139(8)	116(16)	106.6(5.3)	113(3)
170	168	126.86(53)	147(8)	128(19)	113.6(5.7)	120(14) ^c
173	172	41.46(24)	53(4)	41(10)	37.1(1.9)	40(1)
172	171	76.27(27)	85(4)		68.3(3.4)	71(1)
171	170	42.90(25)	54(4)	41(10)	38.3(1.9)	42(1)
174	173	51.64(25)	61(4)		46.2(2.3)	49(1)
173	171	117.72(50)				110(2) ^c

^aCombined analysis of optical, x-ray, and muonic isotope shifts.

^bOnly optical isotope shifts.

^cValue calculated using results from Ref. [82].

$\delta\langle r^2 \rangle^{A,A'} = \lambda^{A,A'} / 0.941$. Table VIII presents the differences in mean-square charge radii arising from this work and previous works. The tabulated $\delta\langle r^2 \rangle^{A,A'}$ values for Yb in Ref. [84] are calculated using semiempirical mass-shift and field-shift parameters of $F_{\text{ICL}} = -11.5$ GHz fm^{−2} and $K_{\text{ICL}} = -4.6(1.6)$ THz u [88]. This mass-shift parameter is much larger in magnitude than that calculated in this work and in Ref. [17], leading to the tabulated values being larger than those determined in this work. Allehabi *et al.* [11] also suggested that the tabulated $\delta\langle r^2 \rangle^{A,A'}$ values are too large based on their own nuclear and electronic structure calculations.

VII. KING PLOT AND CLOCK-TRANSITION ISOTOPE SHIFTS

A King plot compares the isotopic shifts of one transition, α , against those of another, β . By scaling the isotope shift with the reciprocal of the nuclear mass parameter, one defines the *modified* isotope shift,

$$\xi_\alpha^{A,A'} = \delta\nu_\alpha^{A,A'} / \mu^{A,A'}. \quad (10)$$

From Eq. (5) and assuming the nuclear parameters $\lambda^{A,A'}$ and $\mu^{A,A'}$ are the same for both transitions, one finds

$$\xi_\alpha^{A,A'} = (F_\alpha / F_\beta) \xi_\beta^{A,A'} + (K_\alpha - K_\beta F_\alpha / F_\beta). \quad (11)$$

A plot of $\xi_\alpha^{A,A'}$ versus $\xi_\beta^{A,A'}$ should thus, to first order, form a straight line with slope F_α / F_β and intercept $K_\alpha - K_\beta F_\alpha / F_\beta$, known as a King plot. A King plot constructed from the measured isotope shifts for the clock and ICL transitions in Yb I is presented in Fig. 3. With only three isotopes having frequency measurements for the clock transition, only two independent data points can be used to create the King plot (the 171–174 pairing makes it overdetermined). The gradient and intercept for the linear “fit” are 1.0138(12) and −0.102(22) THz u, respectively, where the uncertainties are derived from the square roots of the diagonal entries of the covariance matrix for the fit parameters. This fit was calculated using an orthogonal distance regression [89] due to uncertainties in both abscissa and ordinate values.

TABLE VIII. Differences in mean-square nuclear charge radii $\delta\langle r^2 \rangle^{A,A'}$, determined from the $\lambda^{A,A'}$ values in Table VII via $\delta\langle r^2 \rangle^{A,A'} = \lambda^{A,A'}/0.941$ [81] (in units of 10^{-3} fm^2 , third column). Data from other works are presented for comparison.

A	A'	This work	Ref. [83]	Ref. [82]	Ref. [84] ^a	Ref. [81]	Ref. [11] ^b
176	174	94.4(0.5)	84.8(4.6)	90(2)	115.9(0.1)	114(30)	97(1)
174	172	98.9(0.6)	88.8(4.6)	95(3)	120.7(0.2)	118(28)	102(1)
172	170	126.6(0.6)	113.5(6.6)	119(4)	147.9(0.2)	151(36)	130(1)
170	168	134.8(0.6)	121.0(7.2)	125(15)	156.1(0.4)	160(126)	138(1)
173	172	44.1(0.3)		42(2)	55.6(0.2)	52(19)	
172	171	81.1(0.3)		75(2)	90.7(0.2)		
171	170	45.6(0.3)		44(2)	57.2(0.2)	55(80)	
174	173	54.9(0.3)		51(2)	65.1(0.2)		
173	171	125.1(0.6)		116(3)	146.3(0.2)		

^aReference [84] presents only statistical errors in the uncertainty; the large uncertainty in the mass-shift parameter used in the calculation is not propagated through. Propagating the uncertainty from the mass-shift parameter leads to an uncertainty of $\sim 9 \times 10^{-3} \text{ fm}^2$ for the first row.

^bUncertainty is taken to be $1 \times 10^{-3} \text{ fm}^2$ as the difference between the two (purely computational) methods.

The gradient is given as $F_{\text{ICL}}/F_{\text{clock}}$, and the intercept is given as $K_{\text{ICL}} - K_{\text{clock}}F_{\text{ICL}}/F_{\text{clock}}$. The calculated values in Table IV produce a gradient of 1.0095(28) and an intercept of 0.01(11) THz u. The gradient and intercept values are not inconsistent with those obtained from the King plot in Fig. 3 (experimental).

The unknown isotope shifts for the $^1S_0 - ^3P_0^o$ clock transition can be estimated in three different ways:

(1) Energy-level differences for each isotope are found through MCDHF-CI computations. From these, the isotope shifts are evaluated, and because there is a consistent offset from experimental isotope-shift values in $^1S_0 - ^3P_0^o$, they can be scaled to match the three known experimental isotope shifts.

(2) The mass-shift and field-shift parameters calculated using RIS4 are used with the ICL isotope shifts presented in Table VI to estimate the clock-transition isotope shifts. This method relies heavily on theoretical calculations.

(3) The modified frequency shifts are extrapolated from a King plot constructed using the clock and ICL transitions

and converted back into isotope shifts. This method is based predominantly on experimental measurements.

The estimated isotope shifts for the clock transition for each method are presented in Table IX.

Method 1. The *ab initio* isotope shifts calculated for the clock transition using MCDHF-CI computations, presented in Table II, are larger than experimental values by $\sim 11\%$ (for all the isotopes). This difference we attribute to a systematic effect in the calculations, likely due to the chosen correlation model, which we can account for by a scaling factor. Accounting for the difference leads to the estimates given in the ‘‘Method 1’’ column in Table IX. The adjusted isotope shift between ^{173}Yb and ^{174}Yb is -554 MHz , and that between ^{171}Yb and ^{173}Yb is -1251 MHz , at differences from experiment of 0.5% and -0.7% , respectively. In line with these values we place uncertainties of 1% on the remaining shifts in Table IX (method 1). We regard this as the least reliable estimate of the unmeasured clock-line isotope shifts.

Method 2. Equation (5) applies for both the clock and ICL transitions, with the nuclear parameters taken to be independent of the electronic states. Substituting for $\lambda^{A,A'}$ between these two equations leads to

$$\delta\nu_{\text{clock}}^{A,A'} = \left(K_{\text{clock}} - \frac{F_{\text{clock}}}{F_{\text{ICL}}} K_{\text{ICL}} \right) \mu^{A,A'} + \frac{F_{\text{clock}}}{F_{\text{ICL}}} \delta\nu_{\text{ICL}}^{A,A'}. \quad (12)$$

TABLE IX. Clock-transition isotope shifts $\delta\nu_{\text{clock}}^{A,A'}$ (in MHz) determined using three different methods, as outlined in the text.

A	A'	Method 1	Method 2	Method 3
176	174	-949(10)	-945.1(7.3)	-949.5(2.8)
174	172	-1002(11)	-990.7(7.5)	-995.0(2.9)
172	170	-1272(13)	-1273.0(8.0)	-1275.3(3.3)
170	168	-1347(14)	-1356.0(8.2)	-1357.9(3.4)
173	172	-448(5)	-440.0(3.7)	-443.0(1.4)
172	171	-803(9)	-817.5(4.2)	-816.7(2.0)
171	170	-469(5)	-455.5(3.8)	-458.5(1.5)
174	173	-554(6)	-550.6(3.8)	-552.0(1.5)
173	171	-1251(13)	-1257.6(7.9)	-1259.8(3.3)

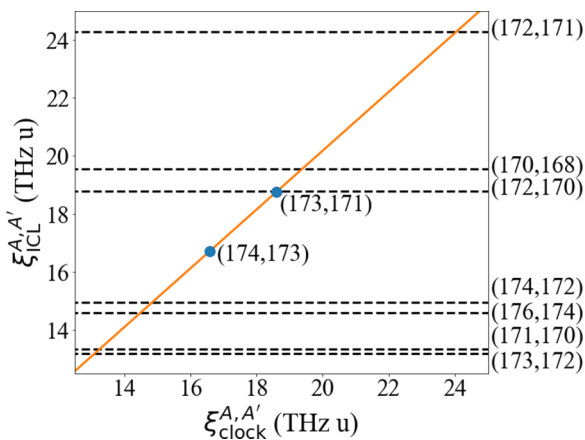


FIG. 3. King plot for clock and intercombination lines of Yb I. Blue circles represent isotope pairs (A, A') with clock-transition measurements. Dashed black lines represent isotope pairs (A, A') without clock-transition measurements. The solid orange line is the King linearity relationship. Error bars are smaller than the marker size.

The ICL isotope shifts presented in Table VI can be used with the calculated mass-shift and field-shift parameters to arrive at the clock-transition isotope shifts. This is equivalent to constructing a King plot using the theoretical mass and field shifts computed using RIS4 and nuclear charge parameters presented in Table VII and leads to the isotope shifts presented in the “Method 2” column of Table IX. The uncertainties are again dominated by the uncertainties in the K parameters for each transition, similar to those for Table VII.

Method 3. Assuming King linearity holds, the King plot in Fig. 3 can be extrapolated to arrive at the clock-transition isotope shifts for other isotope pairs. These estimates are presented in the final column of Table IX. We emphasize that the King plot is based on experimental values and not MCDHF-CI calculations. The only computational component is that of the higher-order hyperfine shifts affecting the centers of gravity. Consistent with this, the uncertainties for method 3 are less than those of method 1. The values in the last two rows of this column provide a consistency check since these are the isotopes used to construct the King plot—they agree within the uncertainties. For comparison, the experimental values appear in Table VI. The presented uncertainties for method 3 are calculated using propagation of errors with the uncertainties from the ICL isotope shifts, nuclear masses, and fit parameters.

The isotope shifts for methods 2 and 3 presented in Table IX provide a region in which experimental searches can be made for the bosonic clock transitions. A weighted mean of the shifts has been used to estimate the absolute clock-transition frequencies, as tabulated in Appendix E. The consistency between results from methods 2 and 3 suggests that method 2 can be used to estimate clock-transition isotope shifts in other divalent atoms with isotope-shift measurements for the $^1S_0 - ^3P_1^o$ ICL transition but not necessarily for the $^1S_0 - ^3P_0^o$ clock transition. For elements with an insufficient number of clock transition frequency measurements across isotopes to construct a King plot, method 2 may be used. Mercury is one such element.

VIII. CONCLUSIONS

Ab initio computations of the isotope shifts for the clock transition and its partnering intercombination line ($^1S_0 - ^3P_1^o$) were performed separately for each stable isotope of Yb using a MCDHF-CI method implemented by the GRASP2018 package [47]. Absolute transition frequency computations agree with experimental results to less than 1% error, while isotope shifts differ from experimental values by 11%. Using these computations, the hyperfine-structure constants for the $^3P_1^o$ state were calculated to within 4% of corresponding experimental values. Corrections for the centroids of the hyperfine manifolds due to the second-order hyperfine interaction in the fermionic isotopes have also been made.

The electronic mass-shift and field-shift parameters were computed with the program RIS4 [46] using the results of the MCDHF-CI computations. The corrected isotope shifts for the intercombination line together with these electronic mass-shift and field-shift parameters enabled computation of the nuclear charge parameters $\lambda^{A,A'}$ consistent with previous

results, but with approximately an order of magnitude reduction in uncertainties. The differences in mean-square charge radii $\delta\langle r^2 \rangle^{A,A'}$ were calculated and found to be significantly smaller than tabulated values of Angeli and Marinova [84].

Experimental isotope shifts for the clock and intercombination lines, corrected for the second-order hyperfine interaction, were used to construct a King plot with two data points. This King plot was used to estimate the unknown isotope shifts for the clock transition in the stable bosonic isotopes. These estimates were found to be reasonably consistent with estimates based on the calculated mass-shift and field-shift parameters.

Similar computations using an alternative method, e.g., CI+MBPT [50], could be performed to provide a theoretical comparison for the computational results of this work. Different nuclear models, including models accounting for the known deformation of Yb nuclei, may also be explored to investigate their potential systematic effects on the computed results.

With suggestions to combine the results of Counts *et al.* [4] with isotope-shift measurements of a clock transition in neutral ytterbium [4,17], the undiscovered bosonic-isotope clock transitions should be sought using the isotope-shift estimates presented in this work (e.g., with cold Yb atoms in an optical lattice trap and a dc magnetic field applied [90]). The clock-transition isotope shift between ^{88}Sr and ^{87}Sr has been measured at the level of tens of millihertz [91,92], and it is foreseeable that levels of precision approaching this could be achieved with ytterbium. Once the clock isotope shifts are identified, King plots can be constructed with other high-precision isotope-shift measurements in neutral and ionized ytterbium in order to investigate King nonlinearity and identify or constrain physics beyond the standard model.

ACKNOWLEDGMENTS

We are grateful for the assistance provided by C. Bording and H. Walker from the UWA High Performance Computing Team. J.S.S. acknowledges support from the University of Western Australia’s Winthrop Scholarship, the John and Patricia Farrant Scholarship, and St Catherine’s College. This research was undertaken with the assistance of resources from the University of Western Australia High Performance Computing Team.

APPENDIX A: NUCLEAR MODEL

The nuclear charge distribution is modeled as a two-component Fermi distribution [93,94]

$$\rho(r) = \frac{\rho_0}{1 + e^{(r-c)/a}}, \quad (\text{A1})$$

where c is the half-density radius, a is related to the nuclear skin thickness t by $t = (4 \ln 3)a$, and ρ_0 is a normalization factor such that

$$\int_0^\infty 4\pi r^2 \rho(r) dr = Z. \quad (\text{A2})$$

For all isotopes the atomic number is $Z = 70$, and the nuclear skin thickness is taken to be $t = 2.18(2)$ fm [57]. This value

TABLE X. Isotope-dependent parameters for the Yb nuclear model. A , mass number; R , rms nuclear charge radius; m , atomic mass. R values are obtained from Ref. [84], and mass values are obtained from Ref. [96], except for ^{168}Yb , which is from Ref. [97].

A	R (fm)	m (u)
168	5.2702(56)	167.93389132(10)
170	5.2853(56)	169.934767246(11)
171	5.2906(57)	170.936331517(14)
172	5.2995(58)	171.936386659(15)
173	5.3046(59)	172.938216215(12)
174	5.3108(60)	173.938867548(12)
176	5.3215(62)	175.942574709(16)

for the nuclear skin thickness is less than the typical value of $t = 2.3$ fm assumed for most nuclei [93]; however, it is the only value found for Yb which includes an explicit uncertainty. Other authors have used $t = 2.3$ fm [82] or $t = 2.4$ fm [95]. The dependence of the results upon the skin thickness was investigated and found to be insignificant. The nuclear parameters used in the MCDHF-CI computations are presented in Table X. In addition to these, the only isotopes with nonzero nuclear spin and magnetic dipole moment are $^{171,173}\text{Yb}$. ^{171}Yb has a nuclear spin of $I = 1/2$ and a magnetic dipole moment of $\mu = 0.49367(1)\mu_N$ [98]. ^{173}Yb has a nuclear spin of $I = 5/2$, a magnetic dipole moment of $\mu = -0.67989(3)\mu_N$ [98], and nuclear electric quadrupole moment of $Q = 2.80(4)$ b [57].

APPENDIX B: STATE COMPOSITIONS

The atomic state functions determined using the MCDHF-CI method consist of weighted combinations of many configuration state functions (CSFs). The percentage contributions of the most significant CSFs are listed for the 1S_0

TABLE XI. The highest contributing CSFs in the compositions of three Yb I atomic states.

CSF	Percentage
	1S_0
$6s^2$	91.56
$6p_+^2$	1.87
$6p_-^2$	1.31
$6s7s$	0.74
$5d_+^2$	0.56
$5d_-^2$	0.35
	$^3P_0^o$
$6s6p_-$	95.60
$5d_-6p_+$	1.02
$6p_-7s$	0.48
	$^3P_1^o$
$6s6p_-$	73.41
$6s6p_+$	22.02
$5d_-6p_+$	0.68
$5d_-6p_-$	0.46
$6p_-7s$	0.38

TABLE XII. Sequences of isotope-shift parameters upon addition of correlation layers. The last row constitutes estimates for the uncertainty in each of the parameters for each isotope. The units for K are GHz u, and the units for F are GHz fm^{-2} .

Layer	K_{clock}	F_{clock}	K_{ICL}	F_{ICL}
$7sp6d5f$	-192.67	-10.4060	-176.48	-10.5151
$8sp7d6f$	-204.07	-10.0544	-189.54	-10.1697
$9sp8d7f$	-282.05	-10.9553	-273.16	-11.0695
$10sp9d8f$	-268.73	-10.9639	-257.58	-11.0710
$11sp10d9f$	-290.47	-10.8480	-281.57	-10.9548
$12sp11d10f$	-288.15	-10.8386	-279.59	-10.9418
$12spdf$	-288.07	-10.8393	-279.55	-10.9425
Uncertainty	2.4	0.0094	2.0	0.013

ground state and the $^3P_{0,1}^o$ excited states in Table XI. Our values are consistent with those reported by Migdalek and Baylis [38], although their calculation extended only to our MR set.

APPENDIX C: UNCERTAINTY ESTIMATES FOR ISOTOPE-SHIFT PARAMETERS

Systematic expansions of the active space and correlation model have been undertaken in order to estimate the uncertainties for the isotope-shift parameters, K and F . The error introduced by truncating the active space at $12spdf$ is estimated by analyzing the K and F values after adding each new correlation layer. This analysis was performed using ^{174}Yb with the same SrD substitutions to account for valence-valence and core-valence correlations as described in Sec. II. The results are presented in Table XII. Based on these results, the uncertainty in the final K and F values due to the truncated active space is estimated to be the absolute difference between the $12sp11d10f$ and $11sp10d9f$ layers, as they were the largest two correlation layers added with an orbital of each symmetry included.

The error introduced by keeping the available core for restricted double substitutions at $4f_{\pm}, 5s, 5p_{\pm}$ is estimated similarly, by analyzing the K and F values with increasingly more core orbitals available for substitutions. This analysis was performed using ^{176}Yb with the active space up to $12spdf$ and SrD substitutions, restricted to at most one substitution from the (varying) available core. The results are presented

TABLE XIII. Sequences of isotope-shift parameters upon inclusion of deeper core-valence correlation. The last row constitutes estimates for the uncertainty in each of the parameters for each isotope. The units for K are GHz u, and the units for F are GHz fm^{-2} .

Available core	K_{clock}	F_{clock}	K_{ICL}	F_{ICL}
$4f$	54.90	-9.4283	56.36	-9.5023
$5p, 4f$	-265.41	-10.5830	-255.65	-10.6681
$5s, 5p, 4f$	-288.05	-10.8326	-279.53	-10.9358
$5s, 4d, 5p, 4f$	-325.22	-10.8255	-315.26	-10.9297
Uncertainty	75	0.015	72	0.013

TABLE XIV. Differences in mean-square nuclear charge radii relative to ^{176}Yb , $\delta\langle r^2 \rangle^{176, A'}$, in units of 10^{-3} fm^2 (second column). Data from other works are presented for comparison.

A'	This work	Ref. [82]	Ref. [84] ^a
174	94.4(0.5)	90(2)	115.9(0.1)
173	149.3(0.8)	142(3)	181.0(0.1)
172	193.4(1.0)	184(5)	236.6(0.1)
171	274.4(1.3)	259(6)	327.3(0.1)
170	320.0(1.6)	303(7)	384.5(0.1)
168	454.8(2.1)	428(13)	540.6(0.3)

^aReference [84] presents only statistical errors in the uncertainty; the large uncertainty in the mass-shift parameter used in the calculation is not propagated through. Propagating the uncertainty from the mass-shift parameter leads to an uncertainty of $\sim 9 \times 10^{-3} \text{ fm}^2$ for the first row.

in Table XIII. Based on these results, this uncertainty is estimated to be twice the absolute difference between the available core used in this paper and the next largest available core of $5s, 4d, 5p, 4f$.

APPENDIX D: ALTERNATIVE PRESENTATION OF DIFFERENCES IN MEAN-SQUARE CHARGE RADII

The differences in mean-square charge radii are presented in Table VIII for pairs of isotopes. Alternatively, a single reference isotope may be chosen, and differences in mean-square

TABLE XV. Estimated (this work) and previously measured clock-transition frequencies in Yb I.

Isotope	Transition frequency (MHz)	Ref.
168	518 297 652.3(3.5)	
170	518 296 294.7(1.4)	
171	518 295 836.59086371(11)	[73]
	518 295 836.59086361(13)	[74]
172	518 295 019.7(1.9)	
173	518 294 576.845268(10)	[75]
174	518 294 025.309217 8(9)	[76]
176	518 293 076.4(2.7)	

charge radii may be given relative to this reference isotope. For ytterbium, this reference isotope is commonly chosen to be ^{176}Yb . Differences in mean-square nuclear charge radii of this type are presented in Table XIV, with the reference isotope of ^{176}Yb .

APPENDIX E: CLOCK-TRANSITION FREQUENCIES

Table XV lists our estimates for the absolute $^1S_0 - ^3P_0^o$ transition frequencies in neutral ytterbium for isotopes where line frequencies have yet to be measured, together with the known frequencies. Our estimates and their uncertainties are based on the weighted mean of the isotope-shift values presented in Table IX using methods 2 and 3 and the existing absolute transition frequency measurements.

- [1] M. S. Safronova, D. Budker, D. DeMille, D. F. Jackson Kimball, A. Derevianko, and C. W. Clark, Search for new physics with atoms and molecules, *Rev. Mod. Phys.* **90**, 025008 (2018).
- [2] V. A. Dzuba, V. V. Flambaum, and S. Schiller, Testing physics beyond the standard model through additional clock transitions in neutral ytterbium, *Phys. Rev. A* **98**, 022501 (2018).
- [3] J.-P. Uzan, The fundamental constants and their variation: Observational and theoretical status, *Rev. Mod. Phys.* **75**, 403 (2003).
- [4] I. Counts, J. Hur, D. P. L. Aude Craik, H. Jeon, C. Leung, J. C. Berengut, A. Geddes, A. Kawasaki, W. Jhe, and V. Vuletić, Evidence for Nonlinear Isotope Shift in Yb^+ Search for New Boson, *Phys. Rev. Lett.* **125**, 123002 (2020).
- [5] J. C. Berengut, D. Budker, C. Delaunay, V. V. Flambaum, C. Frugiuele, E. Fuchs, C. Grojean, R. Harnik, R. Ozeri, G. Perez, and Y. Soreq, Probing New Long-Range Interactions by Isotope Shift Spectroscopy, *Phys. Rev. Lett.* **120**, 091801 (2018).
- [6] C. Frugiuele, E. Fuchs, G. Perez, and M. Schlaffer, Constraining new physics models with isotope shift spectroscopy, *Phys. Rev. D* **96**, 015011 (2017).
- [7] C. Delaunay, R. Ozeri, G. Perez, and Y. Soreq, Probing atomic Higgs-like forces at the precision frontier, *Phys. Rev. D* **96**, 093001 (2017).
- [8] V. A. Yerokhin, R. A. Müller, A. Surzhykov, P. Micke, and P. O. Schmidt, Nonlinear isotope-shift effects in Be-like, B-like, and C-like argon, *Phys. Rev. A* **101**, 012502 (2020).
- [9] V. M. Shabaev, QED theory of the nuclear recoil effect in atoms, *Phys. Rev. A* **57**, 59 (1998).
- [10] S. O. Allehabi, V. A. Dzuba, V. V. Flambaum, A. V. Afanasjev, and S. E. Agbemava, Using isotope shift for testing nuclear theory: The case of nobelium isotopes, *Phys. Rev. C* **102**, 024326 (2020).
- [11] S. O. Allehabi, V. A. Dzuba, V. V. Flambaum, and A. V. Afanasjev, Nuclear deformation as a source of the nonlinearity of the King plot in the Yb^+ ion, *Phys. Rev. A* **103**, L030801 (2021).
- [12] V. V. Flambaum, A. J. Geddes, and A. V. Viatkina, Isotope shift, nonlinearity of King plots, and the search for new particles, *Phys. Rev. A* **97**, 032510 (2018).
- [13] K. Mikami, M. Tanaka, and Y. Yamamoto, Probing new intra-atomic force with isotope shifts, *Eur. Phys. J. C* **77**, 896 (2017).
- [14] Y. V. Stadnik, Probing Long-Range Neutrino-Mediated Forces with Atomic and Nuclear Spectroscopy, *Phys. Rev. Lett.* **120**, 223202 (2018).
- [15] M. Tanaka and Y. Yamamoto, Relativistic effects in the search for new intra-atomic force with isotope shifts, *Prog. Theor. Exp. Phys.* **2020**, 103B02 (2020).
- [16] V. Debierre, C. Keitel, and Z. Harman, Fifth-force search with the bound-electron g factor, *Phys. Lett. B* **807**, 135527 (2020).
- [17] J. C. Berengut, C. Delaunay, A. Geddes, and Y. Soreq, Generalized King linearity and new physics searches with isotope shifts, *Phys. Rev. Res.* **2**, 043444 (2020).
- [18] P.-G. Reinhard, W. Nazarewicz, and R. F. Garcia Ruiz, Beyond the charge radius: The information content of the fourth radial moment, *Phys. Rev. C* **101**, 021301(R) (2020).

- [19] A. Papoulia, B. G. Carlsson, and J. Ekman, Effect of realistic nuclear charge distributions on isotope shifts and progress towards the extraction of higher-order nuclear radial moments, *Phys. Rev. A* **94**, 042502 (2016).
- [20] C. Solaro, S. Meyer, K. Fisher, J. C. Berengut, E. Fuchs, and M. Drewsen, Improved Isotope-Shift-Based Bounds on Bosons beyond the Standard Model through Measurements of the $^2D_{3/2} - ^2D_{5/2}$ Interval in Ca^+ , *Phys. Rev. Lett.* **125**, 123003 (2020).
- [21] J. Rzadkiewicz, Y. Yang, K. Koziol, M. G. O'Mullane, A. Patel, J. Xiao, K. Yao, Y. Shen, D. Lu, R. Hutton, Y. Zou, and JET Contributors, High-resolution tungsten spectroscopy relevant to the diagnostic of high-temperature tokamak plasmas, *Phys. Rev. A* **97**, 052501 (2018).
- [22] K. Koziol and J. Rzadkiewicz, Multiconfiguration Dirac-Hartree-Fock and configuration-interaction study of $4d - 3p$ x-ray transitions in Cu- and Ni-like tungsten ions, *Phys. Rev. A* **98**, 062504 (2018).
- [23] K. T. Cheng, M. H. Chen, W. R. Johnson, and J. Sapirstein, High-precision relativistic atomic structure calculations and the EBIT: Tests of quantum electrodynamics in highly charged ions, *Can. J. Phys.* **86**, 33 (2008).
- [24] L. F. Pašteka, E. Eliav, A. Borschevsky, U. Kaldor, and P. Schwerdtfeger, Relativistic Coupled Cluster Calculations with Variational Quantum Electrodynamics Resolve the Discrepancy Between Experiment and Theory Concerning the Electron Affinity and Ionization Potential of Gold, *Phys. Rev. Lett.* **118**, 023002 (2017).
- [25] T. Kron, R. Beerwerth, S. Raeder, S. Fritzsche, R. Heinke, P. Schönberg, M. Trümper, and K. Wendt, Hyperfine structure study of $^{97,98,99}\text{Tc}$ in a new laser ion source for high-resolution laser spectroscopy, *Phys. Rev. C* **102**, 034307 (2020).
- [26] M. R. Kalita, J. A. Behr, A. Gorelov, M. R. Pearson, A. C. DeHart, G. Gwinner, M. J. Kossin, L. A. Orozco, S. Aubin, E. Gomez, M. S. Safronova, V. A. Dzuba, and V. V. Flambaum, Isotope shifts in the $7s \rightarrow 8s$ transition of francium: Measurements and comparison to *ab initio* theory, *Phys. Rev. A* **97**, 042507 (2018).
- [27] S. Gamrath, P. Palmeri, P. Quinet, S. Bouazza, and M. Godefroid, MCDHF calculations of isotope shifts in neutral antimony, *J. Quant. Spectrosc. Radiat. Transfer* **218**, 38 (2018).
- [28] J. C. Berengut, V. A. Dzuba, and V. V. Flambaum, Isotope-shift calculations for atoms with one valence electron, *Phys. Rev. A* **68**, 022502 (2003).
- [29] R. P. de Groote, S. Kujanpää, Á. Koszorús, J. G. Li, and I. D. Moore, Magnetic octupole moment of ^{173}Yb using collinear laser spectroscopy, *Phys. Rev. A* **103**, 032826 (2021).
- [30] V. A. Dzuba, V. V. Flambaum, and M. G. Kozlov, Fast configuration-interaction calculations for nobelium and ytterbium, *Phys. Rev. A* **99**, 032501 (2019).
- [31] V. A. Dzuba and A. Derevianko, Dynamic polarizabilities and related properties of clock states of the ytterbium atom, *J. Phys. B* **43**, 074011 (2010).
- [32] Z.-M. Tang, Y.-M. Yu, and C.-Z. Dong, Determination of static dipole polarizabilities of Yb atom, *Chin. Phys. B* **27**, 063101 (2018).
- [33] E. Eliav, U. Kaldor, and Y. Ishikawa, Transition energies of ytterbium, lutetium, and lawrencium by the relativistic coupled-cluster method, *Phys. Rev. A* **52**, 291 (1995).
- [34] B. K. Mani and D. Angom, Fock-space relativistic coupled-cluster calculations of two-valence atoms, *Phys. Rev. A* **83**, 012501 (2011).
- [35] C. J. Bostock, D. V. Fursa, and I. Bray, Calculation of electron scattering from the ground state of ytterbium, *Phys. Rev. A* **83**, 052710 (2011).
- [36] S. G. Porsev, Y. G. Rakhlina, and M. G. Kozlov, Calculation of hyperfine structure constants for ytterbium, *J. Phys. B* **32**, 1113 (1999).
- [37] M. G. Kozlov and S. G. Porsev, Combined configuration-superposition and many-particle perturbation calculations for atoms with two valence electrons, *J. Exp. Theor. Phys.* **84**, 461 (1997).
- [38] J. Migdalek and W. E. Baylis, Relativistic transition probabilities and lifetimes of low-lying levels in ytterbium, *J. Phys. B* **24**, L99 (1991).
- [39] J. Migdalek and W. E. Baylis, Correlation effects in a relativistic calculation of the $6s^2 ^1S_0 - 6s6p ^1P_1$ transition in ytterbium, *Phys. Rev. A* **33**, 1417 (1986).
- [40] W. Liu, M. Dolg, and L. Li, Fully relativistic density functional calculations of the ground and excited states of Yb, YbH, YbF, and YbO, *J. Chem. Phys.* **108**, 2886 (1998).
- [41] C. S. Kischkel, M. Baumann, and E. Kummel, Two-photon spectroscopy of some even-parity levels in neutral ytterbium, *J. Phys. B* **24**, 4845 (1991).
- [42] G. Torbohm, B. Fricke, and A. Rosén, State-dependent volume isotope shifts of low-lying states of group-IIa and -IIb elements, *Phys. Rev. A* **31**, 2038 (1985).
- [43] J. Mann and J. Waber, Self-consistent relativistic Dirac-Hartree-Fock calculations of lanthanide atoms, *At. Data Nucl. Data Tables* **5**, 201 (1973).
- [44] R. Silwal, A. Lapierre, J. D. Gillaspay, J. M. Dreiling, S. A. Blundell, Dipti, A. Borovik, G. Gwinner, A. C. C. Villari, Y. Ralchenko, and E. Takacs, Determination of the isotopic change in nuclear charge radius from extreme-ultraviolet spectroscopy of highly charged ions of Xe, *Phys. Rev. A* **101**, 062512 (2020).
- [45] I. P. Grant, Many-electron effects in the theory of nuclear volume isotope shift, *Phys. Scr.* **21**, 443 (1980).
- [46] J. Ekman, P. Jönsson, M. Godefroid, C. Nazé, G. Gaigalas, and J. Bieroń, RIS4: A program for relativistic isotope shift calculations, *Comput. Phys. Commun.* **235**, 433 (2019).
- [47] C. Froese Fischer, G. Gaigalas, P. Jönsson, and J. Bieroń, GRASP2018—A Fortran 95 version of the general relativistic atomic structure package, *Comput. Phys. Commun.* **237**, 184 (2019).
- [48] P. Jönsson, G. Gaigalas, J. Bieroń, C. Froese Fischer, and I. Grant, New version: GRASP2K relativistic atomic structure package, *Comput. Phys. Commun.* **184**, 2197 (2013).
- [49] There is a small incompatibility between RIS4 and GRASP2018 in relation to the ISODATA file, which we overcame by examining the ISODATA file from GRASP2K. RIS4 is written using the GRASP2K architecture and could not be used with GRASP2018 in isolation (it is currently required to operate inside GRASP2K).
- [50] E. Kahl and J. Berengut, AMBIT: A programme for high-precision relativistic atomic structure calculations, *Comput. Phys. Commun.* **238**, 232 (2019).
- [51] M. Safronova and W. Johnson, All-Order Methods for Relativistic Atomic Structure Calculations, in *Advances in Atomic, Molecular, and Optical Physics*, edited by E. Arimondo, P. R.

- Berman, and C. C. Lin (Academic, London, 2008), Vol. 55, pp. 191–233.
- [52] E. Ilyabaev and U. Kaldor, Relativistic coupled-cluster calculations for open-shell atoms, *Phys. Rev. A* **47**, 137 (1993).
- [53] J. Migdalek and W. Baylis, A multiconfiguration Dirac-Fock study of the $6s^2 \ ^1S_0 - 6s6p \ ^3P_1, \ ^1P_1$ transitions in the Yb isoelectronic sequence, *J. Quant. Spectrosc. Radiat. Transfer* **37**, 521 (1987).
- [54] The computation falters when trying to compute the radial wave function for the $13s$ orbital.
- [55] C. Froese Fischer, M. Godefroid, T. Brage, P. Jönsson, and G. Gaigalas, Advanced multiconfiguration methods for complex atoms: I. Energies and wave functions, *J. Phys. B* **49**, 182004 (2016).
- [56] This can be compared with the number of CSFs in the MR in Table I.
- [57] A. Zehnder, F. Boehm, W. Dey, R. Engfer, H. Walter, and J. Vuilleumier, Charge parameters, isotope shifts, quadrupole moments, and nuclear excitation in muonic $^{170-174,176}\text{Yb}$, *Nucl. Phys. A* **254**, 315 (1975).
- [58] D. L. Clark, M. E. Cage, D. A. Lewis, and G. W. Greenlees, Optical isotopic shifts and hyperfine splittings for Yb, *Phys. Rev. A* **20**, 239 (1979).
- [59] I. Grant, *Relativistic Quantum Theory of Atoms and Molecules: Theory and Computation*, Springer Series on Atomic, Optical, and Plasma Physics (Springer, New York, 2007), pp. 11–12.
- [60] J. C. Slater, The theory of complex spectra, *Phys. Rev.* **34**, 1293 (1929).
- [61] G. W. F. Drake, Role of accuracy estimates in atomic and molecular theory, in *7th International Conference on Atomic and Molecular Data and Their Applications - ICAMDATA-2010*, AIP Conf. Proc. No. 1344 (AIP, Melville, NY, 2011), p. 116.
- [62] H.-K. Chung, B. J. Braams, K. Bartschat, A. G. Császár, G. W. F. Drake, T. Kirchner, V. Kokouline, and J. Tennyson, Uncertainty estimates for theoretical atomic and molecular data, *J. Phys. D* **49**, 363002 (2016).
- [63] L. Filippin, R. Beerwerth, J. Ekman, S. Fritzsche, M. Godefroid, and P. Jönsson, Multiconfiguration calculations of electronic isotope shift factors in Al I, *Phys. Rev. A* **94**, 062508 (2016).
- [64] C. Y. Zhang, K. Wang, M. Godefroid, P. Jönsson, R. Si, and C. Y. Chen, Benchmarking calculations with spectroscopic accuracy of excitation energies and wavelengths in sulfur-like tungsten, *Phys. Rev. A* **101**, 032509 (2020).
- [65] P. Palmeri, P. Quinet, and S. Bouazza, MCDHF calculations of isotope shifts of even-parity fine-structure levels in neutral osmium, *J. Quant. Spectrosc. Radiat. Transfer* **185**, 70 (2016).
- [66] C. Froese Fischer and A. Senchuk, Numerical procedures for relativistic atomic structure calculations, *Atoms* **8**, 85 (2020).
- [67] T. Brage, D. S. Leckrone, and C. Froese Fischer, Core-valence and core-core correlation effects on hyperfine-structure parameters and oscillator strengths in Tl II and Tl III, *Phys. Rev. A* **53**, 192 (1996).
- [68] L. Filippin, M. Godefroid, J. Ekman, and P. Jönsson, Core correlation effects in multiconfiguration calculations of isotope shifts in Mg I, *Phys. Rev. A* **93**, 062512 (2016).
- [69] L. Filippin, J. Bieroń, G. Gaigalas, M. Godefroid, and P. Jönsson, Multiconfiguration calculations of electronic isotope-shift factors in Zn I, *Phys. Rev. A* **96**, 042502 (2017).
- [70] Kaya is a Noongar word meaning “hello.”
- [71] Additionally, exploratory computations were performed on a laptop with an Intel Core i7-10510U processor with eight (virtual) cores and 16 GB of RAM, utilizing six cores for computations.
- [72] E. Tiesinga, P. J. Mohr, D. B. Newell, and B. N. Taylor, CODATA recommended values of the fundamental physical constants: 2018, *Rev. Mod. Phys.* **93**, 025010 (2021).
- [73] W. F. McGrew, X. Zhang, H. Leopardi, R. J. Fasano, D. Nicolodi, K. Beloy, J. Yao, J. A. Sherman, S. A. Schäffer, J. Savory, R. C. Brown, S. Römisch, C. W. Oates, T. E. Parker, T. M. Fortier, and A. D. Ludlow, Towards the optical second: Verifying optical clocks at the SI limit, *Optica* **6**, 448 (2019).
- [74] M. Pizzocaro, F. Bregolin, P. Barbieri, B. Rauf, F. Levi, and D. Calonico, Absolute frequency measurement of the $^1S_0 - ^3P_0$ transition of ^{171}Yb with a link to international atomic time, *Metrologia* **57**, 035007 (2020).
- [75] C. Clivati, G. Cappellini, L. F. Livi, F. Poggiali, M. S. de Cumis, M. Mancini, G. Pagano, M. Frittelli, A. Mura, G. A. Costanzo, F. Levi, D. Calonico, L. Fallani, J. Catani, and M. Inguscio, Measuring absolute frequencies beyond the GPS limit via long-haul optical frequency dissemination, *Opt. Express* **24**, 11865 (2016).
- [76] N. Poli, Z. W. Barber, N. D. Lemke, C. W. Oates, L. S. Ma, J. E. Stalnaker, T. M. Fortier, S. A. Diddams, L. Hollberg, J. C. Bergquist, A. Bruschi, S. Jefferts, T. Heavner, and T. Parker, Frequency evaluation of the doubly forbidden $^1S_0 \rightarrow ^3P_0$ transition in bosonic ^{174}Yb , *Phys. Rev. A* **77**, 050501(R) (2008).
- [77] P. E. Atkinson, J. S. Schelphout, and J. J. McFerran, Hyperfine constants and line separations for the $^1S_0 - ^3P_1$ intercombination line in neutral ytterbium with sub-Doppler resolution, *Phys. Rev. A* **100**, 042505 (2019).
- [78] W. H. King, *Isotope Shifts in Atomic Spectra*, Physics of Atoms and Molecules (Plenum, New York, 1984).
- [79] E. C. Seltzer, *K* X-ray isotope shifts, *Phys. Rev.* **188**, 1916 (1969).
- [80] S. A. Blundell, P. E. G. Baird, C. W. P. Palmer, D. N. Stacey, and G. K. Woodgate, A reformulation of the theory of field isotope shift in atoms, *J. Phys. B* **20**, 3663 (1987).
- [81] G. Fricke and K. Heilig, Nuclear charge radii, in *Group I: Elementary Particles, Nuclei and Atoms*, Numerical Data and Functional Relationships in Science and Technology, Vol. 20, edited by H. Schopper (Springer, Berlin, 2004), Chap. 72, pp. 1–10.
- [82] A.-M. Mårtensson-Pendrill, D. S. Gough, and P. Hannaford, Isotope shifts and hyperfine structure in the 369.4-nm $6s - 6p_{1/2}$ resonance line of singly ionized ytterbium, *Phys. Rev. A* **49**, 3351 (1994).
- [83] W.-G. Jin, T. Horiguchi, M. Wakasugi, T. Hasegawa, and W. Yang, Systematic study of isotope shifts and hyperfine structures in Yb I by atomic-beam laser spectroscopy, *J. Phys. Soc. Jpn.* **60**, 2896 (1991).
- [84] I. Angeli and K. Marinova, Table of experimental nuclear ground state charge radii: An update, *At. Data Nucl. Data Tables* **99**, 69 (2013).
- [85] M. Wakasugi, T. Horiguchi, W. G. Jin, Y. Watanabe, and Y. Yoshizawa, The second-order hyperfine perturbation of the optical isotope shift and hyperfine structure in Nd I, *J. Phys. B* **23**, 2173 (1990).

- [86] P. Jönsson, F. A. Parpia, and C. Froese Fischer, HFS92: A program for relativistic atomic hyperfine structure calculations, *Comput. Phys. Commun.* **96**, 301 (1996).
- [87] I. Angeli, A consistent set of nuclear rms charge radii: Properties of the radius surface $R(N,Z)$, *At. Data Nucl. Data Tables* **87**, 185 (2004).
- [88] The sign of this value has been corrected for the difference in sign convention between Ref. [84] and this work.
- [89] P. T. Boggs and J. E. Rogers, Orthogonal distance regression, *Contemp. Math.* **112**, 183 (1990).
- [90] Z. W. Barber, C. W. Hoyt, C. W. Oates, L. Hollberg, A. V. Taichenachev, and V. I. Yudin, Direct Excitation of the Forbidden Clock Transition in Neutral ^{174}Yb Atoms Confined to an Optical Lattice, *Phys. Rev. Lett.* **96**, 083002 (2006).
- [91] T. Takano, R. Mizushima, and H. Katori, Precise determination of the isotope shift of ^{88}Sr - ^{87}Sr optical lattice clock by sharing perturbations, *Appl. Phys. Express* **10**, 072801 (2017).
- [92] S. Origlia, M. S. Pramod, S. Schiller, Y. Singh, K. Bongs, R. Schwarz, A. Al-Masoudi, S. Dörscher, S. Herbers, S. Häfner, U. Sterr, and C. Lisdat, Towards an optical clock for space: Compact, high-performance optical lattice clock based on bosonic atoms, *Phys. Rev. A* **98**, 053443 (2018).
- [93] A.-M. Mårtensson-Pendrill and M. G. H. Gustavsson, The atomic nucleus, in *Handbook of Molecular Physics and Quantum Chemistry*, edited by S. Wilson (Wiley, New York, 2003), Vol. 1, Chap. 30, pp. 477–484.
- [94] B. Hahn, D. G. Ravenhall, and R. Hofstadter, High-energy electron scattering and the charge distributions of selected nuclei, *Phys. Rev.* **101**, 1131 (1956).
- [95] M. Shorifudodoza, M. A. R. Patoary, D. H. Jakubassa-Amundsen, A. K. F. Haque, and M. A. Uddin, Scattering of e^\mp from ytterbium atoms, *Eur. Phys. J. D* **73**, 164 (2019).
- [96] M. Wang, G. Audi, F. G. Kondev, W. Huang, S. Naimi, and X. Xu, The AME2016 atomic mass evaluation (II). Tables, graphs and references, *Chin. Phys. C* **41**, 030003 (2017).
- [97] D. A. Nesterenko, R. P. de Groote, T. Eronen, Z. Ge, M. Hukkanen, A. Jokinen, and A. Kankainen, High-precision mass measurement of ^{168}Yb for verification of nonlinear isotope shift, *Int. J. Mass Spectrom.* **458**, 116435 (2020).
- [98] N. Stone, Table of nuclear magnetic dipole and electric quadrupole moments, *At. Data Nucl. Data Tables* **90**, 75 (2005).